Thermochimica Acta, 86 (1985) 343–350
Elsevier Science Publishers B.V., Amsterdam – Printed in The Netherlands

THE PHASE DIAGRAM OF THE SYSTEM $NaNO_3$–KNO_3 STUDIED BY DIFFERENTIAL SCANNING CALORIMETRY

O. GREIS, K.M. BAHAMDAN and B.M. UWAIS

Department of Chemistry, University of Petroleum and Minerals, Dhahran 31261 (Saudi Arabia)

(Received 24 October 1984)

ABSTRACT

The phase diagram of the binary system $NaNO_3$–KNO_3 has been studied by differential scanning calorimetry (DSC). The liquidus curve has its minimum at 494 K and 50 mol% KNO_3 with a very flat solidus curve. This behavior, however, is only pseudo-eutectic since the subsolidus phase is a solid solution of $NaNO_3$ and KNO_3 over the full composition range. The structure of this solid solution has the space group $R\bar{3}m$ and therefore $NaNO_3$ ($R\bar{3}c$), stable below 548 K, is excluded from it. This result differs from that of earlier investigations. The $R\bar{3}m$ solid solution has its eutectoid point at 382 K and 75 mol% KNO_3. At lower temperatures, heating produces an $\alpha \rightarrow \beta$ phase transition, while a $\beta \rightarrow \gamma \rightarrow \alpha$ transformation is observed on cooling. This is analogous to pure KNO_3, where $\alpha \rightarrow \beta$ occurs at 404 K, $\beta \rightarrow \gamma$ at 391 K, and $\gamma \rightarrow \alpha$ at 353 K.

INTRODUCTION

Alkali nitrates, and especially sodium and potassium nitrates, are important and inexpensive industrial chemicals with applications in many fields and technologies. Some of their mixtures also show very interesting properties such as low melting temperatures. Furthermore, they are chemically stable and non-corrosive to many common structural materials up to about 650 K. Thus, they have been used as heat transfer media for many years, e.g., HTS, HTS_1, HTS_2, HITEC, etc. (HTS stands for heat transfer salts, while HITEC is a DuPont trade name). More recently, such mixtures have also been proposed as promising systems for heat storage and transfer in large solar thermal–electric power plants [1–3]. In view of these applications, phase diagrams of $NaNO_3$–KNO_3 and related systems are of great importance, especially with respect to liquidus and solidus curves, eutectic points and other minimum melting temperatures.

Additionally, the subsolidus regions of such phase diagrams are of considerable interest to crystal chemists. Alkali nitrates, like ammonium nitrate, have a variety of modifications with closely related, ordered and disordered

0040-6031/85/$03.30

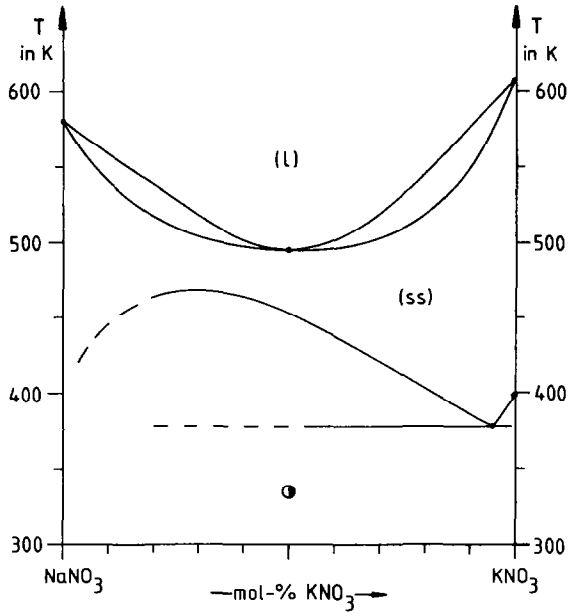

Fig. 1. Phase diagram for the system $NaNO_3$–KNO_3 based on previously published data.

structures, similar to those displayed by alkaline earth carbonates—another family of compounds of the ABX_3 type with complex anions such as NO_3^-, CO_3^{2-}, BO_3^{3-}, etc. Though transformation temperatures for the different modifications of the constituent alkali nitrates are well known and commonly used for calibration in thermal analyses, little analogous data for binary ANO_3–$A'NO_3$ systems are available.

We are studying, as part of a larger project, the crystal chemistry of ABX_3 compounds and ABX_3–$A'BX_3$ systems. The results of our thermal investigations on the system $NaNO_3$–KNO_3 are reported in this paper and compared with literature data. About a dozen phase studies exist on the system $NaNO_3$–KNO_3 [4–17]. In Fig. 1, we present a phase diagram of this system based on the most reliable thermal studies so far available (see also Fig. 1 of ref. 16). The results of the earlier investigations are often not in good agreement and are sometimes even contradictory. Many of these discrepancies may result from the difficulties in achieving equilibrium in the subsolidus region. Therefore, special emphasis has been given to differences observed between the results obtained by heating and cooling.

EXPERIMENTAL

Chemically pure $NaNO_3$ (No. 7418 from Merck or S-343 from Fisher) and KNO_3 (AnalaR from BDH) were used as constituent compounds for the mixtures. Pre-annealing of the pure nitrates above 400 K did not alter their weight, indicating that no significant humidity was absorbed.

The thermal analyses were carried out on a DuPont 990 thermal analyzer using their so-called DSC-cell (differential scanning calorimetry). The samples (~ 20 mg) were placed either in open or hermetically sealed aluminum pans. Visible corrosion of aluminum could not be observed even after ten runs up to 650 K. In a few experiments, hermetically sealed gold pans were used instead of aluminum ones and the same results were obtained. This indicated that thermal analyses on the system $NaNO_3$–KNO_3 could be carried out in aluminum pans without corrosive interference. Calcium difluoride in a sealed aluminum pan served as the reference material. The instrument was calibrated against benzoic acid (m.p. 395.5 K), ammonium nitrate (t.p. 398.4 K), indium (m.p. 429.7 K), ammonium nitrate (m.p. 442.7 K), silver nitrate (m.p. 485.1 K), tin (m.p. 505.0 K), sodium sulfate (t.p. 510.0 K), zinc (m.p. 692.6 K), silver sulfate (t.p. 705.0 K), and quartz (t.p. 846.0 K). The resulting correction curve for the observed sample temperature was non-linear, ranging between $\Delta T = +8$ K at 350 K and $\Delta T = +2$ K at 600 K. In most cases, a temperature correction of $\Delta T = +3$ K was applied for the solidus and liquidus curves and $\Delta T = +2$K for the subsolidus region. The first-order transition temperatures were taken to be those indicated by the intersections of the baselines with straight lines extrapolated from the sloping side of the peaks (so-called extrapolated onset technique, see ref. 26). In the case of second-order transitions and the formation of solid solutions on heating or their reverse reactions on cooling (phase separations), we prefered to accept the temperatures indicated by the maxima of the peaks.

At least three successive runs were carried out for each sample. Generally, the results of the third run were in agreement with those of the second run (indicating equilibrium conditions) and only such data are reported here. An optimal reproducibility and well-pronounced peaks were obtained with heating and cooling rates of 10 K min^{-1}. No significant differences were observed between the results obtained when the substances were studied in open and in closed systems. Thus, the influence of moisture and air is negligible, and pre-annealing of the mixtures is superfluous.

RESULTS AND DISCUSSION

Liquidus and solidus curves

First, the liquidus curve was established by cooling the melts after they were held about 20 K above their melting points for at least 5 min. Very sharp exothermal peaks were observed for $NaNO_3$, KNO_3, and the 0.5 $NaNO_3 \cdot 0.5$ KNO_3 mixture at 576, 605, and 490 K, respectively. The corresponding peaks occurred at 579, 608, and 493 K, respectively, in several successive heating runs. We attributed these small differences to supercooling effects, and therefore corrected all first-order liquidus and solidus data

from cooling runs in the temperature range 480–610 K by adding $\Delta T = +3$ K. All solidus data from cooling and heating runs and all liquidus data from cooling runs are listed in Table 1 and are graphically displayed in Figs. 2 and 3. Our data agree very well with the results of Kramer and Wilson [16], who also observed a much flatter solidus curve than had been reported previously. This behavior, however, is only pseudo-eutectic since (1) the liquidus curve has a well-pronounced curvature rather than a sharp kink at the minimum, and (2) the subsolidus phase is a solid solution (ss) of $NaNO_3$ and KNO_3 over the full range of composition (at least at temperatures close to the solidus curve). The nature of the solid solution has been studied by

TABLE 1

Variable temperatures in the system $NaNO_3$–KNO_3

mol% KNO_3	Liquidus cooling (K)	Solidus cooling (K)	Solidus heating (K)	λ_{max} heating (K)	λ_{max} cooling (K)
0.0	579		579	548	543
1.3	577			541	540
2.5	575			536	538
5.0	570			523	530
6.3	568			515	$R\bar{3}m \rightarrow R\bar{3}c$
7.5	566			506	468
10.0	561			496	461
12.5	556			$R\bar{3}c \rightarrow R\bar{3}m$	454
15.0	551		502	490	451
20.0	542	499	495	486	441
25.0	533	496	494	481	428
30.0	523	496	493	471	416
35.0	514	495	494	461	404
40.0	504	494	494	458	396
45.0	497	494	494	446	386
50.0	494	494	493	435	374
55.0	497	493	494	421	361
60.0	502	494	494	412	
65.0	516	495	494	401	
67.5	522	496	494	397	
70.0	528	496	494	392	
75.0	542	496	494	$Pmcn \rightarrow R\bar{3}m$	
80.0	555	498	495	386	$R\bar{3}m \rightarrow R3m$
85.0	568	502	496	390	361
90.0	583	509	497	394	372
92.5	589		501	396	376
95.0	596			399	381
97.5	602			401	386
98.7	606			403	389
100.0	608		608	404	391

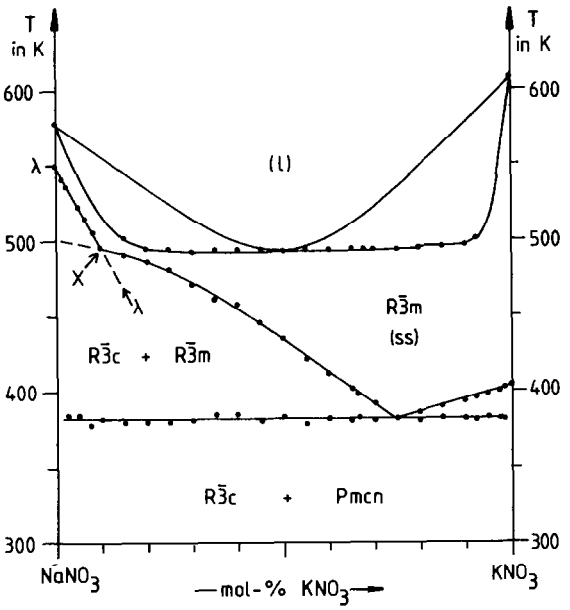

Fig. 2. Phase diagram for the system $NaNO_3$–KNO_3 (DSC, heating rate 10 K min^{-1}).

Tamann and Ruppelt [9] and by Kofler [13] using high-temperature optical microscopy and thermal analyses. From their results, a diphasic subsolidus region can be excluded unambiguously.

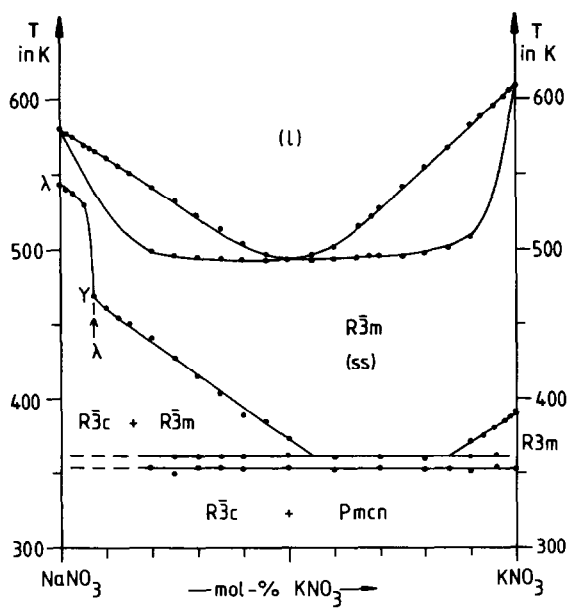

Fig. 3. Phase diagram for the system $NaNO_3$–KNO_3 (DSC, cooling rate 10 K min^{-1}).

Subsolidus phases from DSC heating runs

Though the existence of this solid solution is commonly accepted nowadays, a serious problem exists as far as the structural chemistry at an atomic level is concerned. From room temperature up to about 550 K [18], sodium nitrate crystallizes in the space group $R\bar{3}c$ ($a = 5.071$ Å and $c = 16.825$ Å, hexagonal setting with $Z = 6$, at 298 K [19]), while potassium nitrate crystallizes in the space group $R\bar{3}m$ ($a = 5.425$ Å and $c = 9.836$ Å, hexagonal setting with $Z = 3$, at 424 K [20]) from 404 K up to its melting point at 608 K. The structure of this so-called KNO_3-I or β-KNO_3 modification [20], with complete disorder between two different orientations of the NO_3^--groups, can be considered as the basis structure [21,22] of the room-temperature form of $NaNO_3$, an ordered calcite-type structure. This relationship is analogous to the case of $BaCO_3$-II ($R\bar{3}m$) and $CaCO_3$ ($R\bar{3}c$) [23], another example of strong resemblance in the crystal chemistry of nitrates and carbonates with ABO_3 formula.

One might conclude from Fig. 1 that the solid solution (ss) covers the full range between $NaNO_3$ (450–581 K) and KNO_3 (404–608 K) with a maximum in the miscibility gap at about 25 mol% KNO_3. This, however, is impossible since the two constituent phases have a different structure as expressed by their space groups. On the other hand, the thermal data have so far not been very well established on the $NaNO_3$-rich side of the phase diagram. Thus, the well-documented high-temperature modification of $NaNO_3$ with space group $R\bar{3}m$ ($a = 5.07$ Å and $c = 8.41$ Å, hexagonal setting with $Z = 3$ [24]), stable in the temperature range 550–581 K [18], is not included in the $NaNO_3$-rich region of the diagram at all. It is this phase, however, which has an atomic structure analogous to KNO_3-I—a necessary requirement for the formation of a solid solution of $NaNO_3$ and KNO_3 over the full range of composition.

The results of our DSC studies of the subsolidus region of the system $NaNO_3$–KNO_3 are somewhat simpler in the case of heating runs and we shall discuss them first. The $R\bar{3}m$ solid solution (ss) is characterized by the following boundaries (see Table 1 and Fig. 2): the solidus curve (a), the temperature ordinate 404–608 K for KNO_3 (b), the straight line between the eutectoid point at 382 K and the 404 K phase transition of pure KNO_3 (II → I or $\alpha \rightarrow \beta$) (c), the slightly curved joining line between the eutectoid point at 382 K to point X at 10 mol% KNO_3 and 496 K (d), the connecting line between X and the maximum of the second-order or λ-transition at 548 K for pure $NaNO_3$ (e), and the temperature ordinate 548–579 K for $NaNO_3$ (f). The curvature of (d) can be explained by the kinetically hindered formation of the $R\bar{3}m$ solid solution (ss) at lower temperatures. An extrapolation to pure $NaNO_3$ would result in an intersection at about 506 K, a temperature well within the λ-transition of $NaNO_3$, which begins at about 473 K. In the region of 0–10 mol% KNO_3, however, the λ-transition (e) is so

intense and dominant that curve (d) is covered and masked by overlapping.

Thus, the above structural problem has been solved: the $R\bar{3}m$ solid solution (ss) is formed by the two constituent phases, $NaNO_3$ and KNO_3, both having the same structure with space group $R\bar{3}m$, and $NaNO_3$ with the space group $R\bar{3}c$ is completely excluded. It should be added that below the non-variable eutectoid line at 382 K only a diphasic region could be observed between $NaNO_3$ ($R\bar{3}c$) and KNO_3-II (or α-KNO_3, aragonite-type structure with space group *Pmcn*, $a = 5.412$ Å, $b = 9.157$ Å, $c = 6.421$ Å, $Z = 4$, at 298 K [25]).

Subsolidus phases from DSC cooling runs

The subsolidus region of the $NaNO_3$–KNO_3 phase diagram is quite different, if established from DSC cooling runs (see Table 1 and Fig. 3): they obviously do not represent the true equilibrium, at least at lower temperatures. The shape of the solid solution (ss) region has changed; actually, its area has been increased mainly due to kinetic hindrance in the formation of the diphasic region stable at lower temperatures, which causes a significant shift of the boundaries (c) and (d) towards lower temperatures. Thus, these two curves no longer intersect at the eutectoid line, which is also lowered but to a lesser degree (now at 361 K). Naturally, the intersection, *Y*, of curves (d) and (e) (*X* in Fig. 2) is now at 5 mol% KNO_3 and 468 K.

Another result, also new with respect to the phase diagram $NaNO_3$–KNO_3, but not unexpected in view of the crystal chemistry of pure KNO_3, is the observation of the solid–solid transition of KNO_3-III (or γ-KNO_3, $R3m$, $a = 5.431$ Å and $c = 9.11$ Å, hexagonal setting with $Z = 3$, at 364 K [20]) into KNO_3-II (or α-KNO_3), observed over almost the entire range of the diagram at 353 K. We found the other solid–solid transition from KNO_3-I (or β-KNO_3) into KNO_3-III (or γ-KNO_3) at 391 K. Curve (c) is now, of course, the boundary between the $R\bar{3}m$ solid solution and the diphasic region $R\bar{3}m + R3m$. The γ- and β-KNO_3 structures are described in detail by Nimmo and Lucas [20], who also give the reason why, on heating, an $\alpha \rightarrow \beta$ transition is observed, but on cooling a $\beta \rightarrow \gamma \rightarrow \alpha$ transformation instead of the expected $\beta \rightarrow \alpha$ occurs. Below the $\gamma \rightarrow \alpha$ transition at 353 K, we found only a diphasic region with the consituent compounds $NaNO_3$ ($R\bar{3}c$) and KNO_3 (*Pmcn*).

Finally, we would like to comment on the use of pure $NaNO_3$ and KNO_3 as reference materials for temperature calibrations in thermal analyses. Based on our experience in this work, we can recommend only the following transitions for calibration with heating and cooling rates of 10 K min^{-1} and 20-mg samples:

(a) $NaNO_3$, melting point at 579 K;

(b) $NaNO_3$, freezing point at 579 K (= 576 K observed plus 3 K for supercooling);

(c) KNO_3, $\alpha \rightarrow \beta$ transition at 404 K (on heating only);
(d) KNO_3, melting point at 608 K;
(e) KNO_3, freezing point at 608 K (= 605 K observed plus 3 K for supercooling).

All other transitions, such as the λ-transition of $NaNO_3$ and $\beta \rightarrow \gamma \rightarrow \alpha$ transitions for KNO_3, have a reproducibility less than ± 1 K. In particular, the $\gamma \rightarrow \alpha$ transition can shift as much as ± 10 K depending upon the kinetics.

ACKNOWLEDGMENT

The authors are very much indebted to Prof. J.D. Macomber for interesting discussions.

REFERENCES

1 M.D. Silverman and J.R. Engel, U.S. Dept. Commerce, ORNL/TM-5682, 1977.
2 L. Radosevich, Sandia Laboratories, SAND-78-8221, 1978.
3 L. Tallerico, Sandia Laboratories, SAND-79-8015, 1979.
4 H.R. Carveth, J. Phys. Chem., 2 (1898) 209.
5 H.D. Hissink, Z. Phys. Chem., 32 (1900) 537.
6 M. Amadori, Atti Ist. Veneto Sci., Lett. Arti, Cl. Sci. Mat. Nat., 72 (1912/13) 451.
7 H.V.A. Briscoe and W.M. Madgin, J. Chem. Soc., 123 (1923) 1613.
8 W.M. Madgin and H.V.A. Briscoe, J. Chem. Soc., 123 (1923) 2915.
9 G. Tamann and A. Ruppelt, Z. Anorg. Allg. Chem., 197 (1931) 65.
10 E. Jänicke, Z. Anorg. Allg. Chem., 259 (1949) 92.
11 A.G. Berman and S.I. Berul, Izv. Akad. Nauk SSSR, Sekt. Fiz.-Khim. Anal., Inst. Obshch. Neorg. Khim., 21 (1952) 178.
12 S.I. Berul and A.G. Bergman, Izv. Sekt. Fiz.-Khim. Anal., Inst. Obshch. Neorg. Khim., Akad. Nauk SSSR, 25 (1954) 233.
13 A. Kofler, Monatsh. Chem., 86 (1955) 643.
14 M.P. Susarov, A.I. Efimov and L.S. Timoshenko, Russ. J. Phys. Chem., 43 (1969) 795.
15 W. Klement, Jr., J. Inorg. Nucl. Chem., 36 (1974) 1916.
16 C.M. Kramer and C.J. Wilson, Thermochim. Acta, 42 (1980) 253.
17 M. Kamimoto, Thermochim. Acta, 49 (1981) 319.
18 O. Inkinen, Ann. Acad. Sci. Fenn., Ser. A, 55 (1960) 1.
19 P. Chevin, W.C. Hamilton and B. Post. Acta Crystallogr., 23 (1967) 455.
20 J.K. Nimmo and B.W. Lucas, Acta Crystallogr., Sect. B, 32 (1976) 1968.
21 O. Greis, Z. Anorg. Allg. Chem., 430 (1977) 175.
22 O. Greis and J.M. Haschke, in K.A. Gschneidner, Jr. and L. Eyring (Eds.), The Handbook of the Physics and Chemistry of Rare Earths, Vol. 5, North Holland Publishing Company, Amsterdam, 1982, pp. 387–460, especially p. 412.
23 O. Greis, Crystal chemistry of ordered carbonates with MCO_3 parent structure, Habilitation Colloquium, University of Heidelberg, 1980.
24 G.L. Paul and A.W. Pryor, Acta Crystallogr., Sect. B, 27 (1971) 2700.
25 J.K. Nimmo and B.W. Lucas, J. Phys. C, 6 (1973) 201.
26 G. Lombardi, For Better Thermal Analysis, ICTA-Information, 2nd edn., Stablimento Tipolitografico Ugo Pinto, Rome, 1980.